Polyhedron 201 (2021) 115164

Contents lists available at ScienceDirect

Polyhedron

journal homepage: www.elsevier.com/locate/poly

# A new zinc(II) complex with $N_2O_2$-tetradentate schiff-base derived from pyridoxal-S-methylthiosemicarbazone: Synthesis, characterization, crystal structure, DFT, molecular docking and antioxidant activity studies

Qumars Poladian [a], Onur Şahin [b], Tuncay Karakurt [c], Berat İlhan-Ceylan [a], Yasemin Kurt [a,*]

[a] Department of Chemistry, Engineering Faculty, Istanbul University-Cerrahpasa, 34320 Istanbul, Turkey
[b] Department of Occupat Health & Safety, Faculty of Health Sciences, Sinop University, TR-57000 Sinop, Turkey
[c] Department of Chemical and Process Engineering, Faculty of Engineering-Architecture, Kırsehir Ahi Evran University, 40100 Kırsehir, Turkey

ARTICLE INFO

*Article history:*
Received 16 January 2021
Accepted 13 March 2021
Available online 19 March 2021

*Keywords:*
Pyridoxal
Thiosemicarbazone
X-ray crystallography
DFT
Molecular docking

ABSTRACT

A new unsymmetrical $N_2O_2$-tetradentate Schiff-base complex of zinc(II) was synthesized by the template reaction of pyridoxal-S-methylthiosemicarbazone and 2-hydroxy-4-methoxy-benzaldehyde as starting compounds. S-methylthiosemicarbazone (1) and zinc(II) complex [Zn(L)$CH_3OH$] (**2**) were characterized by elemental analysis, FT-IR, UV–visible, $^1H$, and $^{13}C$ NMR spectra. The molecular structure of the complex (**2**) was determined by single crystal X-ray diffraction technique. The structure consists of a distorted square-pyramidal geometry around the central metal, Zn(II). Quantum chemical calculations were carried out using density functional theory DFT/B3LYP, 6–31G (d), and LanL2DZ basis sets for theoretical characterization of the compounds. The experimental and theoretical data were compared comprehensively. The potential energy distribution (PED) analysis was performed for the assignment of vibration frequencies. In order to support in vitro studies, molecular docking studies have been carried out so that the title compound can be an inhibitor of Epidermal Growth Factor Receptor (1 m17), and the relationship between calculated HOMO energies and docking studies has been examined. In addition, the total antioxidant capacity (as TEAC value) and free radical scavenging activity of the compounds were determined by Cupric Reducing Antioxidant Capacity (CUPRAC) and 1,1-diphenyl-2-picryl hydrazyl (DPPH) methods, respectively.



## 1. Introduction

Thiosemicarbazones are an important class of Schiff base ligands that have been studied for a considerable period of time for their biological properties [1]. Thiosemicarbazones and also their metal-based complexes present a great variety of biological activities ranging from antitumor [2,3], antiviral [4], antibacterial [5], and antioxidant [6] activities. The biological activity of thiosemicarbazones is related to parent aldehyde or ketone groups and the substitution of N or S atoms, as well as their chelating ability with transition metal ions [7,8].

Heterocyclic molecules are well known as key structural components of many pharmaceutical drugs. Thiosemicarbazones derived from heteroaromatic carbonyls are pharmacologically active compounds [9,10]. Currently, thiosemicarbazone derivatives such as marboran or triapine are already used in medical practice [11,12].

Pyridoxal, containing a heterocyclic pyridine ring, is one of the forms of vitamin $B_6$ [13]. Vitamin $B_6$ is an essential micronutrient for living organisms. Deficiency symptoms include dermatitis, microcytic hypochromic anemia, impaired immune function, depression, confusion, and convulsions in humans. Its active form, pyridoxal 5′-phosphate, serves as a coenzyme in many enzyme reactions in amino acid, glucose, and lipid metabolism [14]. In addition, Vitamin B6 may directly or indirectly play a role in oxidative stress and the antioxidant defense system. It can quench reactive oxygen species (ROS) [15]. Thiosemicarbazones derived from pyridoxal and their metal complexes have drawn special interest in the past few decades due to their interesting chemical and biological properties [16-18].

Zinc is the second most prominent trace metal in the human body after iron and plays an important role in various biological systems. Zinc(II) complexes of thiosemicarbazones which exhibit

* Corresponding author.
*E-mail address:* dasdemir@istanbul.edu.tr (Y. Kurt).

https://doi.org/10.1016/j.poly.2021.115164
0277-5387/

antimicrobial and antioxidant activity have been reported [19]. It has been also shown that thiosemicarbazone-based Zn(II) complexes are more efficient inhibitors of cancer cell growth [20].

The template reaction of S-alkylthiosemicarbazones in the presence of metal ions involves condensation of thioamide of S-alkylthiosemicarbazones and carbonyl of a ketone or aldehyde. Although, numerous $N_2O_2$-type template complexes with Fe(III) [21], Co(II) [22], Ni(II) [23], VO(IV) [24], Cu(II) [25], Mn(III) [26] ions have been investigated, a relatively small number of studies have been reported on $N_2O_2$-type Zn(II) complexes with bis(arylidene)-S-alkyl-thiosemicarbazones [27-30]. According to our knowledge, $N_2O_2$-type template complexes of $N^1$,$N^4$-bis(arylidene)-S-alkyl-thiosemicarbazone ligands which containing pyridoxal moiety have not been studied yet.

In this study, a new Zn(II) complex (**2**) of $N_2O_2$ chelating thiosemicarbazone ligand (**L**) was synthesized by the template reaction of pyridoxal-S-methyl-thiosemicarbazone (**1**) and 2-hydroxy-4-methoxy-benzaldehyde in the presence of Zn(II) acetate (Fig. 1). The starting ligand (**1**) and Zn(II) complex (**2**) were characterized by analytical and spectroscopic methods. The crystal structure of the complex was determined by X-ray diffraction. The geometric data, fundamental vibrational modes, $^1$H, $^{13}$C NMR chemical shifts, and electronic characteristics have been calculated by using DFT/B3LYP method to support experimental results. Furthermore, molecular docking studies were also carried out to find out the mode of action of the title compound towards the molecular target Epidermal Growth Factor Receptor (1 m17). Antioxidant activity of the starting ligand (**1**) and Zn(II) complex (**2**) was determined with CUPric Reducing Antioxidant Capacity (CUPRAC) and DPPH radical scavenging activity assays [31,32].

## 2. Experimental

### 2.1. Materials and physical measurements

All reagents and solvents used in the study were of reagent grade and used as commercially purchased without further purification. The elemental analyses were determined on a Thermo Finnigan Flash EA 1112 Series Elemental Analyzer. FT-IR data were obtained by an Agilent Cary 630 spectrophotometer with an Attenuated Total Reflectance (ATR) unit in the 4000–600 $cm^{-1}$ range. UV–Vis spectra of the compounds, spectrophotometric antioxidant capacity and activity measurements were performed by a Shimadzu 2600 UV–Vis Spectrometer using a pair of matched quartz cuvettes of 1 cm thickness. The $^1$H and $^{13}$C NMR spectra were recorded on Bruker Avance-500 model spectrometer relative to $SiMe_4$ using DMSO $d_6$.

### 2.2. X-Ray diffraction analysis

Suitable crystal of **2** was selected for data collection which was performed on a SuperNova, diffractometer equipped with a graphite-monochromatic Mo-$K_\alpha$ radiation at 296 K. The H atoms of C atoms were located from different maps and then treated as riding atoms with C—H distances of 0.93–0.97 Å. The other H atoms were located in a difference map refined freely. We used these procedures for our analysis: solved by direct methods; SHELXS-2013 [33]; refined by full-matrix least-squares methods; SHELXL-2013 [34]; molecular graphics: MERCURY [35]; solution: WinGX [36].

### 2.3. Theoretical calculations

Molecular modeling of the complex (**2**) was carried out with the Gaussian 09 program [37] using the basic functional density theory DFT/B3LYP [38,39] with 6–31G (d) [40] basis set for the C, N, O, H atoms and with LanL2DZ [41-43] basis set for Zn(II) metal atom. The potential energy distribution (PED) analysis in the assignments of the vibrational frequencies was calculated using the VEDA 4 software [44]. The PyRx [45] program containing the Autodock vina [46] software with Lamarckian genetics was used as the scoring algorithm for molecular docking virtual scanning process was used in Discovery Studio Visualizer 2020 [47] to show receptor-ligand interactions.

### 2.4. Antioxidant capacity and activity tests

The CUPRAC method, as described by the method of Apak et al., [31] is based on the reduction of a cupric neocuproine complex (Cu (II)–Nc) by antioxidants to the yellow-orange colored cuprous chelate (Cu(I)–Nc). The reaction mixture of Cuprac antioxidant capacity consisted of $CuCl_2{\cdot}2H_2O$ (1 mL, 10 mmol), Nc (1 mL, 7.5 mmol), $NH_4Ac$ buffer solution pH 7 (1 mL, 1.0 M), x mL synthesized compound, and $H_2O$ (1.1–x mL) respectively. After that, the mixture (4.1 mL) was incubated at room temperature. After 30 min. of incubation, the absorbance was recorded at 450 nm against reagent blank from another 30 min. The calibration curves (absorbance Vs concentration graphs) of the ligand and the complex were plotted under the described conditions, and their Trolox Equivalent Antioxidant Capacities (TEAC coefficients) [ε(each component)/ε (trolox); ε molar absorptivity] were calculated. The assay was repeated three times in order to determine the statistical errors. The obtained data are given as averaged value ± standard deviation (SD).

The DPPH (2,2-di(4-*tert*-octylphenyl)-1-picrylhydrazyl) radical scavenging activity of the compounds was determined by the method of Brand-Williams et al. with minor modifications [32]. The solutions were added to the test tube in the order of 2 mL of 0.1 mM DPPH, x mL of sample solution at different concentration and 2–x mL methanol. The mixture, which had a total volume of 4 mL, was shaken vigorously and incubated in the dark for 30 min. The decrease in absorbance of the resulting solution was then measured spectrophotometrically at 515 nm against methanol. The FRS activity was calculated as the percentage of DPPH decolorization using the equation: FRS (%) = $[(A_0–A_S)/A_0] \times 100$, where $A_0$ is the absorbance of the control DPPH, and $A_S$ is the absorbance of the assayed samples.

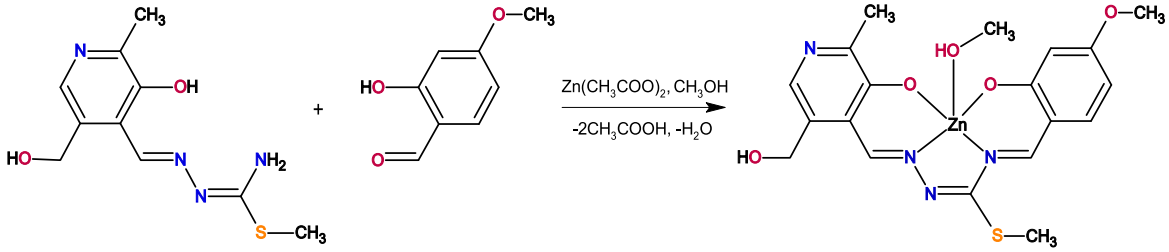


**Fig. 1.** Synthesis of $N_2O_2$ template complex (**2**).

### 2.5. Synthesis of the starting ligand (1)

Pyridoxal S-methyl-thiosemicarbazone (**1**) was prepared with a small modifications of the literature method [48]. To an ethanolic solution (20 mL) of thiosemicarbazide (0.5 g, 6 mmol) was added methyl iodide (0.6 mL, 8 mmol) and refluxed for 3 h. Pyridoxal hydrochloride (1.6 g, 8 mmol) was added to this solution and continued to heat for another 3 h. The final solution was neutralized with a sufficient amount of aqueous $NaHCO_3$ solution (%5, w/w). The paleyellow precipitate was collected by filtration and washed with 5 mL water and dried in vacuo over $P_2O_5$.

**1 :** Paleyellow, m.p. 205–206 °C, yield 72.2%, Anal. Calcd for $C_{10}H_{14}N_4O_2S$ (254.31 g.mol$^{-1}$): C, 47.23; H, 5.55; N, 22.03; S, 12.61. Found: C, 47.01; H, 5.38; N, 21.81; S,12.42%. UV–Vis [DMF, $\lambda_{max}$, nm (log ε)]: 230 (3.91), 316 (4.28), 350 (4.27), $365_{sh.}$ (4.21). FT-IR (selected bands, cm$^{-1}$): $\nu(NH_2)_{as.}$ 3364, $\nu(NH_2)_{s.}$ 3347, ν(OH) 3319, $\delta(NH_2)$ + ν(C = N$^1$) $1654_{br}$, ν(N$^2$ = C) 1586, δ(OH) 1376, ν (C—S) 751. $^1$H NMR (DMSO $d_6$, 500 MHz, 25 °C, ppm):12.24, 11.72 (cis/trans ratio: 1/3, s, 1H, $OH_{phen.}$), 8.70, 8.57 (syn/anti ratio: s, 1H, C*H* = N), 7.97, 7.89 (s, 1H, pyr-C*H*), 7.22 (s, 2H, $NH_2$), 5.31 (d, *J* = 5.22 Hz, 1H, $CH_2OH$), 4.58 (s, 2H, $CH_2$), 2.48, 2.40 (*cis/trans* ratio: 1/1, *s*, 3H, S–$CH_3$), 2.38, 2.32 (s, 3H, pyr–$CH_3$). $^{13}$C NMR (DMSO $d_6$, 126 MHz, 25 °C, ppm): 167.58, 151.16, 148.62, 147.18, 138.97, 132.37, 121.30, 59.19, 19.31, 13.05.

### 2.6. Synthesis of Zn(II) complex (2)

The solution of pyridoxal S-methylthiosemicarbazone (0.25 g, 1 mmol) and 2-hydroxy-4-methoxy-benzaldehyde (0.15 g, 1 mmol) in 10 mL methanol was added dropwise on the solution of $Zn(CH_3COO)_2{\cdot}2H_2O$ (0.2 g, 1 mmol) in 5 mL methanol. The mixture was left to stand at room temperature for a few days. The resulting orange crystals washed with a mixture of methanol/ether (1:1, 5 mL) and dried in air [27].

**2:** Orange crystal, m.p. > 350 °C, yield 17%, Anal. Calcd for $C_{19}H_{22}N_4O_5SZn$ (483.87 g. mol$^{-1}$): C, 47.16; H, 4.58; N, 11.58; S, 6.63. Found: C, 47.25; H, 4.76; N, 11.78; S, 6.50%. UV–Vis [DMF, $\lambda_{max}$, nm (log ε)]: 264 (4.12), 335 (4.51), 413 (4.32), 463 (4.23). FT-IR (selected bands, cm$^{-1}$): ν($CH_2OH$) 3293, ν(C = N$^1$) 1615, ν (N$^2$ = C) 1585, ν(N$^4$ = C) 1523, ν(N—N) 1024, ν(C—S) 784. $^1$H NMR (DMSO $d_6$, 500 MHz, 25 °C, ppm): δ 8.98 (s, 1H, CH = N$^1$), 8.50 (s, 1H, C*H* = N$^4$), 7.44 (s, 1H, pyr-C*H*), 7.38 (d, *J* = 9.0 Hz, 1H, c), 6.28 (d, *J* = 2.44 Hz, 1H, a), 6.24 (dd, *J* = 2.44 Hz, *J* = 8.79 Hz, 1H, b), 5.25 (t, *J* = 5.29 Hz, 1H, $CH_2OH$), 4.56 (d, *J* = 5.23 Hz, 2H, $CH_2$-OH), 4.08 (q, *J* = 5.24 Hz, 1H, $CH_3OH$), 3.80 (s, 3H, O-$CH_3$), 3.17 (d, *J* = 5.28 Hz, 3H, $CH_3OH$) 2.60 (s, 3H, S-$CH_3$), 2.40 (s, 3H, Pyr-$CH_3$). $^{13}$C NMR (DMSO $d_6$, 126 MHz, 25 °C, ppm): 177.69, 168.05, 164.09, 163.35, 162.95, 158.00, 155.26, 139.38, 133.89, 131.61, 117.33, 113.96, 107.75, 104.60, 60.07, 55.92, 29.48, 21.27, 13.09.

## 3. Results and discussion

The template reaction of pyridoxal S-methyl-thiosemicarbazone (**1**) with 2-hydroxy-4-methoxy benzaldehyde in the presence of Zn(II) metal salt in 1:1:1 M ratio leads to the formation of Zn(II) complex as shown in Fig. 1. The complex (**2**) was in expected chemical composition, [Zn(**L**)$CH_3OH$], as **L** is a dibasic N$^1$,N$^4$-bis(ariliden)thiosemicarbazidato ligand. The thiosemicarbazone ligand (**1**) is soluble in common organic solvents such as methanol, ethanol, DMF, and DMSO but sparingly soluble in chloroform. The orange-colored template complex, stable in air, is soluble in DMF and DMSO but sparingly soluble in protonated organic solvents.

**Table 1**
Crystal data and structure refinement parameters for **2**.

| | |
|---|---|
| Empirical formula | $C_{19}H_{22}N_4O_5SZn$ |
| Formula weight | 483.83 |
| Crystal system | Triclinic |
| Space group | *P*-1 |
| *a* (Å) | 8.4093 (6) |
| *b* (Å) | 9.4792 (5) |
| *c* (Å) | 14.5613 (6) |
| α (°) | 77.119 (4) |
| β (°) | 89.377 (4) |
| γ (°) | 67.044 (6) |
| *V* (Å$^3$) | 1038.16 (11) |
| Z | 2 |
| $D_c$ (g cm$^{-3}$) | 1.548 |
| μ (mm$^{-1}$) | 1.32 |
| θ range (°) | 4.1–27.9 |
| Measured refls. | 14,995 |
| Independent refls. | 4872 |
| $R_{int}$ | 0.058 |
| S | 1.07 |
| R1/w*R*2 | 0.040/0.102 |
| $\Delta\rho_{max}/\Delta\rho_{min}$ (eÅ$^{-3}$) | 0.68/-0.38 |

**Table 2**
Selected bond distances and angles (Å,°).

| | | | |
|---|---|---|---|
| N1-Zn1 | 2.1175(19) | N3-Zn1 | 2.076(2) |
| O1-Zn1 | 1.9823(17) | O3-Zn1 | 1.9616(16) |
| Zn1-O5 | 2.063(2) | | |
| O3-Zn1-O1 | 101.18(7) | O3-Zn1-O5 | 100.21(8) |
| O1-Zn1-O5 | 99.95(8) | O3-Zn1-N3 | 88.48(7) |
| O1-Zn1-N3 | 153.12(8) | O5-Zn1-N3 | 102.94(8) |
| O3-Zn1-N1 | 155.05(9) | O1-Zn1-N1 | 87.47(7) |
| O5-Zn1-N1 | 101.27(8) | N3-Zn1-N1 | 74.46(7) |

**Table 3**
Hydrogen bond parameters (Å, °).

| D-H···A | D-H | H···A | D···A | D-H···A |
|---|---|---|---|---|
| C10—H10A···O1$^{i}$ | 0.96 | 2.46 | 3.412 (3) | 174 |
| C11—H11···O4 | 0.93 | 2.35 | 3.001 (3) | 127 |
| C19—H19C···O4$^{ii}$ | 0.96 | 2.58 | 3.413 (4) | 146 |
| O4—H4A···O1$^{iii}$ | 0.97 (3) | 1.81 (3) | 2.773 (3) | 171 |
| O5—H5A···N4$^{iv}$ | 0.83 (3) | 1.83 (3) | 2.653 (3) | 172 |

Symmetry codes: (i) x − 1, y + 1, z; (ii) − x + 1, −y + 3, −z + 1; (iii) − x + 1, −y + 2, −z + 1; (iv) − x + 2, −y + 2, −z + 1.

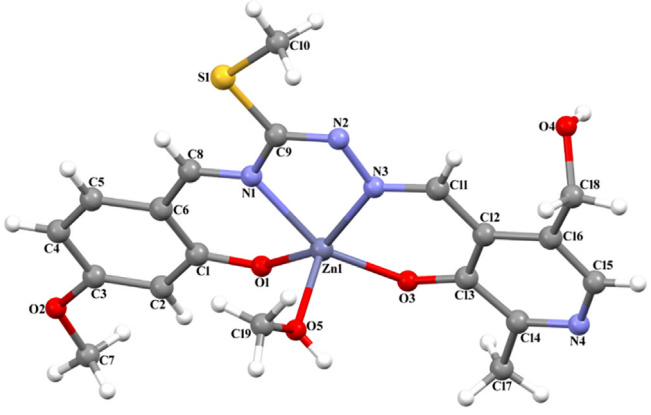


**Fig. 2.** The molecular structure of **2** showing the atom numbering scheme.

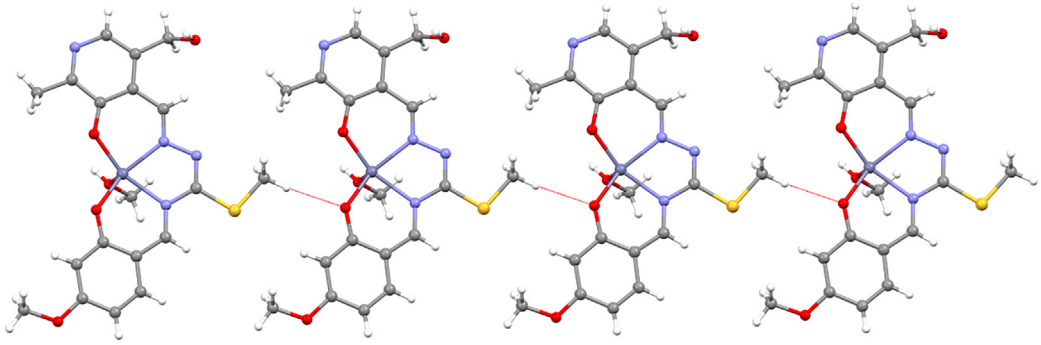

**Fig. 3.** The 1D supramolecular network in **2**.

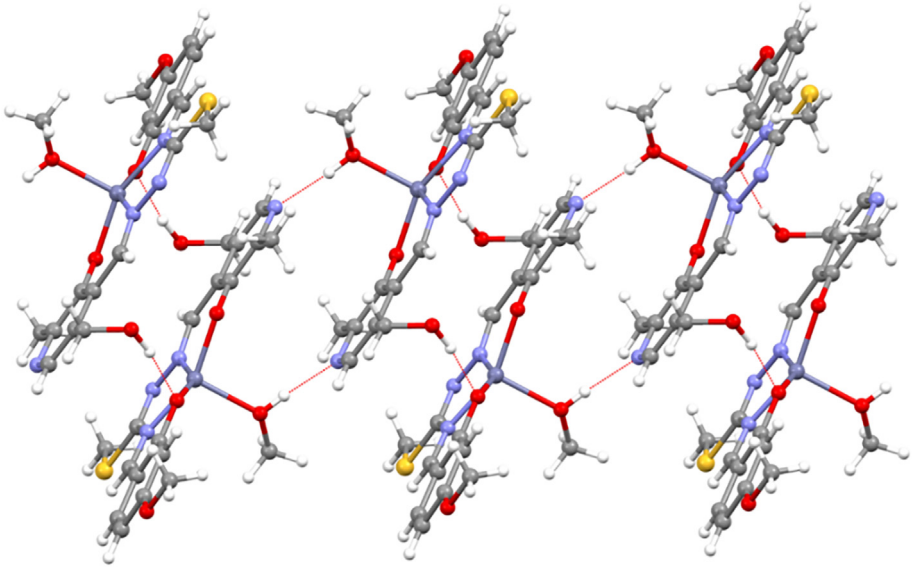

**Fig. 4.** The formation of edge-fused $R_2^2(14)$ and $R_2^2(18)$ rings in **2**.

### 3.1. X-ray crystallography

A suitable single crystal of Zn(II) complex (**2**) was obtained by slow evaporation of the methanol solution. Crystal data and structure refinement parameters of **2** are given in Table 1. Selected bond distances and angles are presented in Table 2, and hydrogen bond parameters are given in Table 3.

The molecular structure of the Zn(II) complex, [Zn(L)$CH_3OH$] **(2)**, with the atom numbering scheme, is shown in Fig. 2. The asymmetric unit of **2** contains one Zn(II) ion, one $N^1$-{[3-hydroxy-5-(hydroxymethyl)-2-methylpyridin-4-yl]methylidene}-$N^4$-[(2-hydroxy-4-methoxyphenyl)methylidene]-S-methyl-thiosemicarbazone (**L**) formed as a result of the template condensation, and one methanol ligand. The Zn(II) ion is coordinated by two oxygen atoms [Zn1-O1 = 1.9823(17) Å and Zn1-O3 = 1.9616 (16) Å] and two nitrogen atoms [Zn1-N1 = 2.1175(19) Å and Zn1-N3 = 2.076(2) Å] from (**L**) and an oxygen atom [Zn1-O5 = 2.063(2) Å] from methanol ligand [28,30]. The geometry of the Zn1 atom can be evaluated by the Addison distortion index tau ($\tau = (\beta-\alpha)/60$, where $\alpha$ and $\beta$ are the two largest coordinated angles in the complex). In a five-coordinate geometry, $\tau = 0$ for a square pyramidal geometry and $\tau = 1$ for a trigonal bipyramidal geometry. The $\tau$ value is calculated as 0.03 and this value shows that Zn1 atom has a distorted square pyramidal geometry. The C10 atom in the molecule at (x, y, z) acts as hydrogen-bond donor to the O1 atom in the molecule at (x-1, y + 1, z), so forming a C(7) chain which is running parallel to the [1 1 0] direction (Fig. 3). The O4 atom in the molecule at (x, y, z) acts as hydrogen-bond donor to the O1 atom in the molecule at (1-x, 2-y, 1-z), so forming a centrosymmetric $R_2^2(18)$ ring centered at (1/2, 1, 1/2). Similarly, the O5 atom in the molecule at (x, y, z) acts as hydrogen-bond donor to the N4 atom in the molecule at (2-x, 2-y, 1-z), so forming a centrosymmetric $R_2^2(14)$ ring centered at (1, 1, 1/2). The combination of these hydrogen bonds produces edge-fused $R_2^2(14)R_2^2(18)$ rings, which are running parallel to the [1 0 0] direction (Fig. 4). The combination of O—H···O, C—H···O and O—H···N hydrogen bonds (Table 3) generating a 2D supramolecular network.

### 3.2. Theoretical calculations

#### 3.2.1. FT–IR spectra

The experimental and calculated FT–IR spectra of Zn(II) complex (**2**) are shown in Fig. S1 and detailed PED assignments are shown in Table 4. All calculated vibration frequencies scaled by 0.9613. [49]

The template condensations of the S-methylthiosemicarbazones and aldehydes can be easily monitored by comparing the IR spectra of S-methylthiosemicarbazone and the Zn(II) com-

**Table 4**
Comparison of the Experimental and Calculated Vibrational Spectra of Zn(II) complex (**2**).

| Experimental FT-IR, $cm^{-1}$ | Calculated (Unscaled)FT-IR ($cm^{-1}$) | Calculated (Scaled)FT-IR ($cm^{-1}$) | Assignments with PED, % |
|---|---|---|---|
| | 3809 | 3662 | νOH (100) |
| 3292 m | 3689 | 3546 | νOH (100) |
| | 3241 | 3116 | νCH (99) |
| | 3228 | 3103 | νCH (97) |
| 3080 vw | 3188 | 3065 | τHCCC1 + νCH (48) |
| | 3178 | 3055 | νCH 97 |
| | 3176 | 3053 | νCH (55) + νCH (21) + νCH (24) |
| | 3171 | 3048 | νCH (99) |
| 3043 vw | 3161 | 3039 | νCH (99) |
| 3019 vw | 3158 | 3036 | $\nu CH_3$ (*asym*) (89) |
| | 3158 | 3036 | $\nu CH_3$ (*asym*) (85) |
| | 3157 | 3035 | $\nu CH_3$ (*asym*) (82) + $\nu CH_3$ (*asym*) (11) |
| | 3112 | 2992 | $\nu CH_3$ (*asym*) (55) + $\nu CH_3$ (*asym*) (44) |
| | 3099 | 2979 | $\nu CH_3$ (*asym*) (50) + $\nu CH_3$ (*asym*) (50) |
| 2978vw | 3098 | 2978 | $\nu CH_3$ (*asym*) (58) + $\nu CH_3$ (*asym*) (40) |
| | 3091 | 2971 | νCH (99) |
| 2965vw | 3079 | 2960 | $\nu CH_3$ (45) + $\nu CH_3$ (28) + $\nu CH_3$ (28) |
| 2956w | 3074 | 2955 | $\nu CH_2$ (*asym*) (89) + $\nu CH_2$ (*asym*) (10) |
| 2935w | 3046 | 2928 | $\nu CH_3$ (16) + $\nu CH_3$ (31) + $\nu CH_3$ (54) |
| 2924w | 3042 | 2924 | $\nu CH_3$ (36) + $\nu CH_3$ (13) + $\nu CH_3$ (50) |
| 2915w | 3032 | 2915 | $\nu CH_3$ (11) + $\nu CH_3$ (44) + $\nu CH_3$ (44) |
| 2831w | 3016 | 2899 | $\nu CH_2$ (11) + $\nu CH_2$ (89) |
| 1615 s | 1676 | 1611 | νCC (27) + νOC (13) + νCC (12) + νCC (11) |
| | 1659 | 1595 | νNC (31) + νNC (11) |
| 1585 s | 1644 | 1580 | νNC (18) + νNC (21) + νCC (10) + δHCC (12) |
| | 1623 | 1560 | νNC (21) + νCC (37) + δCCC (10) |
| 1523w | 1573 | 1512 | νNC (19) + νOC (14) + νCC (12) |
| | 1559 | 1499 | νNC (10) + νOC (12) |
| 1483 s | 1545 | 1485 | νNC (19) |
| | 1532 | 1473 | νNC (12) + νOC (10) + δHCC (14) + δHCH (10) |
| | 1524 | 1465 | δHCH (83) |
| | 1520 | 1461 | δHCH (61) + δHCH (11) + τHCOZn (10) + τHCOZn (11) |
| 1456w | 1514 | 1455 | δHCH (13) + δHCH (14) + δHCH (47) + τHCOC (10) |
| | 1509 | 1451 | δHCH (40) + δHCH (29) + τHCOZn (15) |
| | 1507 | 1449 | νOC (12) + νOC (16) δHCH (15) |
| | 1503 | 1445 | δHCH (39) + δHCH (38) + τHCOC (16) |
| 1438vw | 1495 | 1437 | νNC (15) + δHCN (12) + δHCH (11) |
| | 1490 | 1432 | δHCH (15) + δHCH (33) + δHCH (24) |
| | 1486 | 1428 | δHCH (42) + δHCH (38) + τHCCC (14) |
| | 1484 | 1427 | δHCH (50) + τHCSC (10) |
| | 1481 | 1424 | δHCH (28) |
| 1417 s | 1476 | 1419 | δHCH (15) + δHCH (16) + δHCH (11) |
| | 1468 | 1411 | δHCH (36) + δHCH (38) + τHCSC (17) |
| 1398w | 1462 | 1405 | νOC (27) + νNC (13) |
| | 1430 | 1375 | νCC (14) + νCC (10) |
| 1368w | 1427 | 1372 | δHOC (20) + δHCO (16) + τHCCC (13) |
| | 1418 | 1363 | δHCC (13) + δHCH (11) + δHCH (11) |
| | 1413 | 1358 | νNC (15) + δHCC (41) |
| | 1411 | 1356 | δHCC (25) |
| | 1382 | 1329 | δHOC (53) + τHCOZn (14) |
| | 1371 | 1318 | δHCH (33) + δHCH (33) + δHCH (21) |
| 1312 s | 1369 | 1316 | δHOC (18) + δHCO (10) + τHCCC (29) |
| | 1357 | 1304 | νOC (12) + δHCC (17) |
| 1297w | 1352 | 1300 | νNC (10) + νCC (12) |
| | 1330 | 1279 | δCNC (10) + δCCC (11) + τHCCC (12) |
| 1257w | 1300 | 1250 | νCC (10) + νNC (11) + δHCN (47) |
| 1241w | 1288 | 1238 | νCC (22) + νOC (31) + δHCC (14) |
| | 1285 | 1235 | νCC (10) + νCC (20) + νNC (18) + δHCC (18) |
| 1213w | 1250 | 1202 | νCC (14) + δHCC (38) |
| 1198 s | 1240 | 1192 | νNC (43) + νCC (13) |
| | 1208 | 1161 | δHCH (14) + τHCOC (28) + τHCOC (26) |
| 1155 s | 1205 | 1158 | δHOC (22) + δHCO (32) + τHCCC (15) + τHCCC (12) |
| | 1201 | 1155 | νCC (11) + νNC (28) |
| | 1184 | 1138 | δHCH (13) + δHCH (12) + τHCOZn (12) + τHCOZn (52) + τHCOZn (10) |
| 1126w | 1176 | 1130 | δHCH (14) + δHCH (14) + τHCOC (37) + τHCOC (17) + τHCOC (18) |
| | 1155 | 1110 | νCC (13) + δHCC (13) + δHCC (43) |
| 1083w | 1118 | 1075 | δHOC (23) + τHCOZn (18) + τHCOZn (23) |
| 1024 s | 1107 | 1064 | νNN (16) + νCC (16) |
| | 1074 | 1032 | νNN (16) |
| | 1062 | 1021 | νCC (11) + νOC (68) |
| | 1053 | 1012 | νOC (10) + νOC (71) |
| | 1053 | 1012 | νOC (17) + νOC (22) + τHCCC (12) + τHCCC (11) |
| | 1052 | 1011 | νOC (38) + τHCCC (10) + (11) |

(*continued on next page*)

**Table 4** (*continued*)

| Experimental FT-IR, $cm^{-1}$ | Calculated (Unscaled)FT-IR ($cm^{-1}$) | Calculated (Scaled)FT-IR ($cm^{-1}$) | Assignments with PED, % |
|---|---|---|---|
| 991w | 1033 | 993 | νNN (23) |
| 974w | 1001 | 962 | δHCH (11) + τHCSC (20) + τHCSC (27) |
| 960w | 997 | 958 | νCC (12) + δCCC (13) + δCCC (12) |
| | 994 | 956 | τHCCC (47) |
| | 992 | 954 | δHCH (11) + δHCH (10) + τHCSC (36) + τHCSC (11) + τHCSC (16) |
| | 991 | 953 | τHCSC (17) |
| 947w | 980 | 942 | τHCCC (12) + τHCCC (60) |
| | 960 | 923 | δHCO (10) + τHCCC (10) + τOCCC (14) |
| | 948 | 911 | νCH5 (22) + τHCCC (45) + τHCCC (12) + τCCCC (10) |
| 868w | 898 | 863 | τHCCC (77) |
| | 884 | 850 | νNC (15) + νSC (12) + δNCN (12) + δCNN (12) |
| 833 s | 861 | 828 | τHCCC (49) + τCCCC (12) + γOCCC (18) |
| 819vw | 857 | 824 | δCNC (16) + δCCC (14) + δCCN (14) + δCCC (10) |
| 784 s | 807 | 776 | νCH5 (51) + τHCCC (14) + γOCCC (14) |
| 771w | 796 | 765 | τHCCC (10) + γOCCC (23) |
| 729w | 775 | 745 | νCC (11) + νCC (12) + δNCC (12) + γOCCC (15) |

ν: stretching, δ: in-plane bending, γ: out-of-plane bending, τ: torsion, *asym*: asymmetric stretching

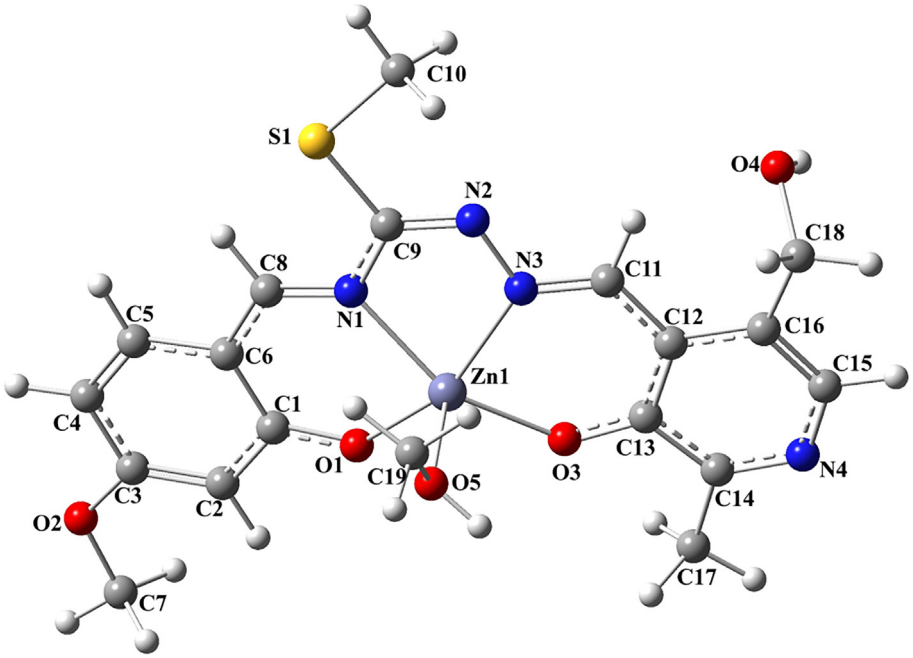


**Fig. 5.** Optimized structure of Zn(II) complex.

plex. In the FT-IR spectrum of pyridoxal S-methylthiosemicarbazone (**1**), the stretching vibration bands of the OH, $N^4H_2$, C = $N^1$, and $N^2$ = C groups were observed as reported previously [50-53]. After complexation, ν(2-OH) and ν($N^4H_2$) bands disappeared in the complex spectrum due to the deprotonation of 2-OH groups and the formation of a new C = $N^4$ band between the thioamide and the second aldehyde [30].

In Schiff-based IR spectra, the vibration peaks of the C=N stretching exhibits high-density bands [54]. In the spectrum of Zn(II) complex (**2**), these stretching bands (C = $N^1$, $N^2$ = C, and C = $N^4$) were experimentally observed as strong and sharp at 1615, 1585, and 1523 $cm^{-1}$ while these bands were calculated at 1594, 1581, and 1512 $cm^{-1}$ [27]. It can be said that these bands shifts to lower frequencies because the lone pair of electrons on the N atom of the imine group is shared to coordinate with the metal atom. Likewise, the reason for the decrease in frequency, the weakening of the C=N bond, which is coordinated with the metal center, with a decrease in π-electron density due to an inductive effect [54].

While the CH stretching bands of benzene and pyridine rings were experimentally observed at 3080–3043 $cm^{-1}$ region and calculated at 3116–3039 $cm^{-1}$. The symmetrical and asymmetrical vibration bands of $CH_3$ were found at 3019–2978 $cm^{-1}$ and 2959–2915 $cm^{-1}$, respectively, while 3036–2978 $cm^{-1}$ and 2960–2915 were calculated. The symmetrical and asymmetrical vibration bands of $CH_2$ were observed at 2956 $cm^{-1}$ and 2931 $cm^{-1}$, respectively, while 2955 and 2899 $cm^{-1}$ were calculated [50]. The O-$CH_3$ and C=C stretching vibration peaks, which

**Table 5**
Experimental and Calculated $^{13}C$ and $^{1}H$ NMR chemical shifts δ(ppm) from TMS for **2.**

| [Zn(L)$CH_3OH$] (**2**) | | | | | |
|---|---|---|---|---|---|
| Atom | Experimental | Calculated | Atom | Experimental | Calculated |
| C9 | 177.69 | 179.33 | H11 | 8.98 | 10.63 |
| C1 | 168.05 | 176.38 | H8 | 8.50 | 8.72 |
| C13 | 164.09 | 175.54 | H15 | 7.44 | 8.49 |
| C3 | 163.35 | 157.17 | H5 | 7.38 | 7.93 |
| C14 | 162.95 | 156.83 | H4 | 6.24 | 7.36 |
| C11 | 158.00 | 152.97 | H2 | 6.28 | 6.55 |
| C8 | 155.26 | 149.39 | H18A | 4.56 | 5.12 |
| C15 | 139.38 | 144.68 | H18B | 4.56 | 4.89 |
| C5 | 133.89 | 128.86 | H7A | 3.80 | 4.55 |
| C16 | 131.61 | 125.22 | H7B | 3.80 | 4.22 |
| C4 | 117.33 | 120.01 | H7C | 3.80 | 4.20 |
| C12 | 113.96 | 119.46 | H10A | 2.60 | 2.74 |
| C6 | 107.75 | 111.79 | H10B | 2.60 | 3.10 |
| C2 | 104.60 | 95.44 | H10C | 2.60 | 3.21 |
| C18 | 60.07 | 53.91 | H17A | 2.40 | 2.40 |
| C7 | 55.92 | 45.93 | H17B | 2.40 | 3.24 |
| C19 | 29.48 | 38.64 | H17C | 2.40 | 3.03 |
| C17 | 21.27 | 15.38 | H19A | 3.17 | 2.70 |
| C10 | 13.09 | 10.71 | H19B | 3.17 | 2.46 |
| | | | H19C | 3.17 | 3.07 |
| | | | H4 | 5.25 | 1.18 |
| | | | H5 | 4.08 | 0.28 |

**Table 6**
Atomic charges (e) of **2** in gas phase and solution phase.

| **Zn(II) complex (2)** | | | |
|---|---|---|---|
| Dimethylformamide (ε = 37.219) | Dimethylsulfoxide (ε = 46.826) | Gas (ε = 1) | |
| C1 | 0.357212 | 0.357055 | 0.367884 |
| C2 | −0.158481 | −0.158619 | −0.146403 |
| C3 | 0.334615 | 0.334605 | 0.334938 |
| C4 | −0.094048 | −0.094182 | −0.080502 |
| C5 | −0.080226 | −0.080233 | −0.076372 |
| C6 | 0.00271 | 0.00258 | 0.013014 |
| C7 | −0.054618 | −0.054663 | −0.047783 |
| C8 | 0.154316 | 0.154464 | 0.142145 |
| C9 | 0.257963 | 0.258052 | 0.249101 |
| C10 | −0.43566 | −0.435669 | −0.435157 |
| C11 | 0.183402 | 0.183564 | 0.172953 |
| C12 | 0.006083 | 0.006128 | 0.006218 |
| C13 | 0.330085 | 0.330141 | 0.327389 |
| C14 | 0.123131 | 0.123152 | 0.123558 |
| C15 | 0.008484 | 0.008422 | 0.019373 |
| C16 | −0.013243 | −0.013148 | −0.020334 |
| C17 | −0.302754 | −0.302857 | −0.294053 |
| C18 | 0.050518 | 0.050488 | 0.053622 |
| C19 | −0.065658 | −0.06566 | −0.066298 |
| N1 | −0.577252 | −0.577269 | −0.576116 |
| N2 | −0.304561 | −0.304714 | −0.291297 |
| N3 | −0.408004 | −0.407933 | −0.416047 |
| N4 | −0.431954 | −0.432324 | −0.39354 |
| O1 | −0.704279 | −0.704603 | −0.675631 |
| O2 | −0.520231 | −0.520312 | −0.510222 |
| O3 | −0.709034 | −0.709319 | −0.687585 |
| S1 | 0.108883 | 0.108935 | 0.11455 |
| O4 | −0.568412 | −0.568644 | −0.544643 |
| O5 | −0.534749 | −0.534885 | −0.521836 |
| **Zn (II)** | **1.071998** | **1.072125** | **1.059862** |
| **L → M** | 0.928002 | 0.927875 | 0.940138 |

are important bands, were calculated at 1021–1011 and 1560–1472 $cm^{-1}$, respectively. The N—N peak was calculated at 1064 $cm^{-1}$ as sharp intensity and observed at 1024 $cm^{-1}$ [55].

### 3.2.2. $^{1}H$ and $^{13}C$ NMR spectra

GIAO (Gauge-Independent Atomic Orbital) [56,57] method was used to determine NMR chemical shift values of the complex structure and TMS [tetramethylsilane, $Si(CH_3)_4$] was taken as reference. The $^{1}H$ and $^{13}C$ NMR chemical shift values calculated by selecting dimethylsulfoxide (DMSO) solvent for TMS are 32.15 and 190 ppm for the DFT/B3LYP/6-31G (d) theorem, respectively. The chemical shifts of $^{1}H$ NMR and $^{13}C$ NMR obtained theoretically using the optimized structure (Fig. 5) of the Zn(II) complex are given in Table 5 comparatively. The corresponding $^{1}H$ and $^{13}C$ NMR spectra of the starting ligand (**1**) are also presented as Supplementary Material (Fig. S2, Table S1).

When the calculated $^{13}C$ NMR spectrum is examined, the highest peak values of the title compound belong to the C9, C1, C13, C3, C8, C11, C14, and C15 atoms, respectively. The chemical shift values of these atoms are higher than those of other carbon atoms due to the high deshielding effect of electronegative N, O and S atoms. The chemical shifts of these atoms were calculated at 179.33, 176.37, 175.54, 157.17, 149.39, 152.97, 156.83, and 144.68 ppm, respectively. Methyl carbon atoms of the complex structure were observed to give high field intensity peaks as expected. It has been calculated that the C7, C10 and C17 atoms give peaks at 45.93, 10.71, and 15.38 ppm, respectively. The chemical shift value of the H11 proton adjacent to the C11 atom of the highest peak in the $^{1}H$ NMR spectrum is seen as a large shift of 10.63 ppm. The experimental NMR spectra of **2** are also given in Fig. S3 and S4.

### 3.2.3. Charge distribution analysis

The calculation of atomic charges is very important in defining the electronic characteristics of molecular systems [58]. The optimized structure of the Zn(II) complex structure is shown in Fig. 5. The calculated Mulliken atomic charges of the atoms forming the complex structure with the Zn(II) metal ion are given in Table 6. It can be seen that the calculated charge on the metal ion is significantly lower than its formal charge + 2 because there is a significant charge transition from O and N atoms to the center Zn(II) metal. Density-of-states (DOS) is an important concept for solid physics, representing the number of states in the unit energy range. In Fig. S5, it is seen that complex structure is mostly composed of s and p atomic orbitals, and the graph shows Total Density-of-states (TDOS). The central Zn(II) metal ion in complex structure has mostly 4 s, 3d, 4p and 5p orbital arrangement and

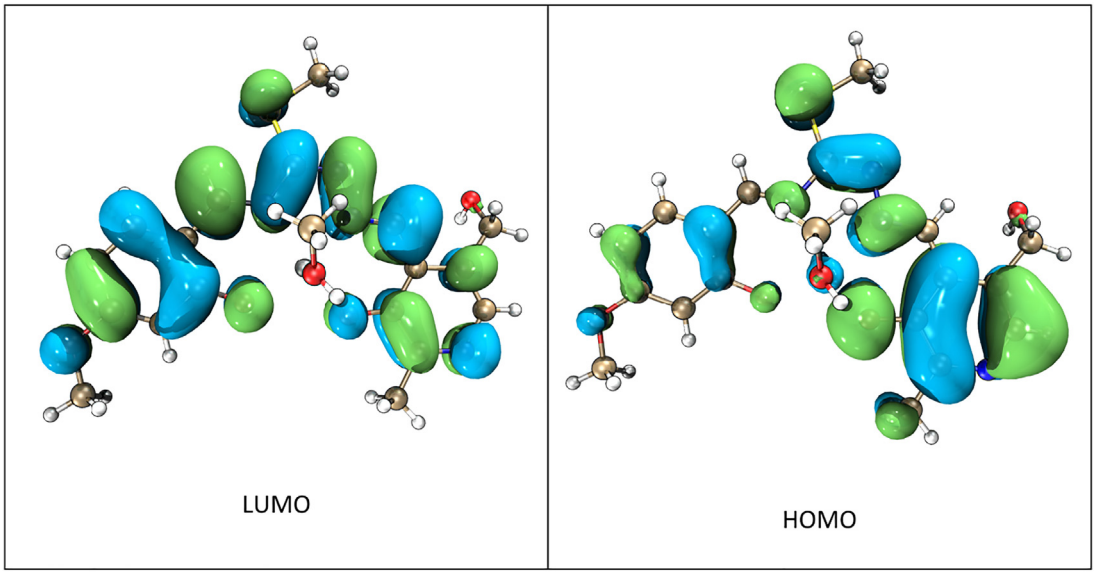


**Fig. 6.** Representation of HOMO-LUMO Frontier orbitals (iso value = 0.002) of Zn(II) complex (**2**).

**Table 7**
Experimental and calculated major absorption wavelength ($\lambda_{max}$), excitation energies (E), Oscillator strength (f), assignment and Excited State of **2** (HOMO = 116; LUMO:117).

| **Major** Excited State and **contributions** | E(eV) | Wavelength (nm) | | Oscillator strength (f) | Assignment |
|---|---|---|---|---|---|
| | | Experimental | Calculated | | |
| Excited state-1 | | | | | |
| 103 → 117(27%) | 5.981 | 265 | 207.31 | 0.1654 | $\pi \rightarrow \pi^*$ |
| 105 → 117(19%) | | | | | |
| 115 → 122(28%) | | | | | |
| Excited state-2 | | | | | |
| 113 → 117(62%) | 3.662 | 335 | 338.58 | 0.3880 | $n \rightarrow \pi^*$ |
| 116 → 118(23%) | | | | | |
| Excited state-3 | | | | | |
| 115 → 117(79%) | 3.089 | 413 | 401.30 | 0.1277 | *MLCT, LMCT, LLCT* |
| 116 → 117(99%) | 2.780 | 464 | 445.29 | 0.3109 | *MLCT, LMCT, LLCT* |

the arrangement of this ion in Zn(II) complex is [core]$4S^{0.30}$ $3d^{9.98}$ $4p^{0.42}$ $5p^{0.01}$. The occupancies of d orbitals are 3dxy $^{1.99678}$ 3dxz $^{1.99659}$ 3dyz $^{1.99465}$ $3dx^2y^{2\,(1.99593)}$ $dz^{2(1.99336)}$. The oxygen and nitrogen atoms of the ligand contribute to the complex formation with 2 s, 2p, 3p, and 3d orbitals while sulfur atom also contributes with 3 s, 3p, 4 s, 3d, and 4p orbitals.

In addition, net charges on the active centers of the metal complex were calculated and it was observed that there was charge transfer from the ligand of the complex to the central metal ion (Table 6). When Table 2 is analyzed, charge transfer from ligand to metal (**L** → **M**) was calculated at 0.940138 for the gas phase, at 0.927875 for DMSO, and 0.928002 for the DMF. It was observed that the charge transfer also increased in the gas phase compared to the DMSO and DMF solvents.

### 3.2.4. Electronic properties

The frontier orbitals (HOMO and LUMO) are also known as electron donor and acceptor groups [59,60]. These can be used to determine the intermolecular charge transfers, as well as many molecular properties such as ionization potential, electron affinity, chemical reactivity, kinetic stability, electronegativity and electrophilicity index can be calculated by considering the HOMO and LUMO energy values [61-63]. The distributions and energy levels of FMOs of the complex structure are shown in Fig. 6. The calculated energy between the HOMO and LUMO gap is 3.14 eV.

UV–Vis spectra of the compounds were determined in $5 \times 10^{-5}$ M DMF solution at room temperature. Experimental and calculated UV–Vis spectra of the complex structure (**2**) in the study are given in Fig. S6.

In the spectrum of the starting ligand (**1**) and its complex (**2**), the absorption bands located at 200–300 nm region are assigned to the $\pi \rightarrow \pi^*$ (C=N) transition of azomethine groups and the $\pi \rightarrow \pi^*$ (C=C) transition in the aromatic rings [51,54].

In both experimental and calculated spectra, 4 major maximum peaks were observed for Zn(II) complex structure. The first major absorption peak was recorded at 265 nm resulted from the $\pi \rightarrow \pi^*$ transitions of the double bonds in the benzene and azomethine groups of the complex structure, which was calculated at 207.82 nm. The second major peak was observed at 336 nm for **2** originates from the $n \rightarrow \pi^*$ transitions of the lone pair orbital electrons on the N atom in the azomethine group, which was calculated at 338.58 nm. The $\pi \rightarrow \pi^*$ transition for Zn(II) complex (**2**) shifts towards higher wavelengths compared to the starting ligand (**1**) while $n \rightarrow \pi^*$ transition appears as a single band at 335 nm. These shifts indicate that the ligand is in coordination with the metal ion [64].

The last two peaks were observed in the complex structure at 413 and 465 nm while calculated at 401.30 and 445.29 nm. The major contributions for these transitions are shown in Table 7. The contributions of the Zn(II) atom plays an important role in molecular orbitals and these contributions; LUMO + 5(0.6%),

**Table 8**
Molecular modeling data for compounds co-ligand and Zn(II) during docking in the active site of enzyme 1 m17.

| Compound | Affinity (kcal/mol) | Name | Distance Donor. . .Acceptor (Å) | Interaction Category | Interaction Types | Donor group | Donor group Types | Acceptor group | Acceptor group Types | HOMO (eV) |
|---|---|---|---|---|---|---|---|---|---|---|
| Co-ligand | −**7.3** | A:MET769:HN - A:AQ4999:O4 | 1.81 | Hydrogen Bond | Conventional Hydrogen Bond | A: MET769: HN | H-Donor | A: AQ4999: O4 | H-Acceptor | |
| | | A:CYS773:HN - A: AQ4999:O2 | 1.97 | Hydrogen Bond | Conventional Hydrogen Bond | A: CYS773: HN | H-Donor | A: AQ4999: O2 | H-Acceptor | −5.60 |
| | | A:AQ4999:H3 - A: ASP831:OD1 | 2.56 | Hydrogen Bond | Conventional Hydrogen Bond | A: AQ4999: H3 | H-Donor | A: ASP831: OD1 | H-Acceptor | |
| | | A:ASP831:OD1 - A:AQ4999 | 3.65 | Electrostatic | Pi-Anion | A: ASP831: OD1 | Negative | A: AQ4999 | Pi-Orbitals | |
| | | A:PHE699 - A: AQ4999 | 3.81 | Hydrophobic | Pi-Pi Stacked | A: PHE699 | Pi-Orbitals | A: AQ4999 | Pi-Orbitals | |
| | | A:PHE699 - A: AQ4999:C1 | 5.08 | Hydrophobic | Pi-Alkyl | A: PHE699 | Pi-Orbitals | A: AQ4999: C1 | Alkyl | |
| **Zn(II)** | −**7.6** | d:RES1:N41 - A: ASP776:OD1 | 5.46 | Electrostatic | Attractive Charge | d:RES1: N41 | Positive | A: ASP776: OD1 | Negative | |
| | | d:RES1:H43 - A: PRO770:O | 2.80 | Hydrogen Bond | Conventional Hydrogen Bond | d:RES1: H43 | H-Donor | A: PRO770: O | H-Acceptor | −5.42 |
| | | A:LEU820:CD1 - d:RES1 | 3.48 | Hydrophobic | Pi-Sigma | A: LEU820: CD1 | C—H | d:RES1 | Pi-Orbitals | |
| | | d:RES1 - A: VAL702 | 5.14 | Hydrophobic | Pi-Alkyl | d:RES1 | Pi-Orbitals | A:VAL702 | Alkyl | |
| | | d:RES1 - A: ALA719 | 5.43 | Hydrophobic | Pi-Alkyl | d:RES1 | Pi-Orbitals | A:ALA719 | Alkyl | |

LUMO + 1(1.9%), LUMO(0.6%), HOMO(2.2%), HOMO-1(1.7%), HOMO-3(0.6%), HOMO-11(1.2%) and HOMO-13(2%), which these orbitals are more intense than ligand's other atoms and may be assigned mainly to LMCT (ligand to metal charge transfer) and MLCT (metal to ligand charge transfer) [65]. It can be said that the other orbitals, where ligand atoms are more intense, maybe assigned mainly to LLCT (ligand to ligand charge transfer) [22]. Due to the complete $d^{10}$ electronic configuration of Zn(II) ion, d-d transitions were not observed [27].

*3.2.5. Molecular docking studies*

In this study, the X-ray crystal structure of the Epidermal Growth Factor Receptor (EGFR) (PDB ID: 1 m17) was used. Epidermal Growth Factor Receptor (EGFR), which signals via tyrosine kinase, is considered one of the most important targets for the development of new anticancer agents [66]. Overexpression of EGFR has been detected in many solid tumors, including lung [67], head-neck [68], ovarian [69], and colon tumors. Before proceeding to the calculations, the crystal structure of 1 m17 and all ligand compounds were prepared using the protein and ligand preparation wizards included in the PyRx package. Before molecular docking, firstly water and heteroatoms other than natural ligand (co-ligand) were removed from the 1 m17 protein structure, and hydrogen atoms and Gasteiger charges were added. The docking scores of Zn(II) complex (**2**) and co-ligand and the interactions between the receptor and ligands and the HOMO energy levels of the ligands are given in Table 8 the docking processes of the target protein to the active binding sites in Figs. 7 and 8.

The ligands were found to bind to the active binding site of the receptors with weak non-covalent interactions, more specifically with hydrogen bonding and alkyl interactions. As seen in Fig. 7, the O and N atoms of the reference co-ligand and the receptor CYS773, MET769, and ASP831 residues of the receptor have 1.97, 1.81, and 2.56 Å length of hydrogen bond interactions, respectively. The Zn(II) complex, on the other hand, interacts with the N atom and the receptor's PRO770 residues with a 2.80 Å long hydrogen bond in Fig. 8. In Table 7, it is seen that the HOMO energy of ligands with high-affinity values is low. As a result, it can be said that the title compound may be an inhibitor candidate for the 1 m17 receptor based on the docking score.

*3.3. Antioxidant studies*

*3.3.1. Trolox equivalent antioxidant capacity assay (CUPRAC)*

According to the CUPRAC method, the Trolox calibration curve was drawn, and the slope of the curve gave the molar absorption coefficient. For the starting thiosemicarbazone (**1**) and the Zn(II) complex (**2**), molar absorption coefficients were calculated under the same conditions. TEAC values of the samples were calculated by dividing the molar absorption coefficient of the tested compound to the molar absorption coefficient of Trolox. The TEAC values of the starting ligand (**1**) and the complex (**2**) were found as 1.33 and 0.85, respectively. The tested thiosemicarbazone ligand has a relatively higher CUPRAC antioxidant capacity compared to the reference Trolox, however, the complex shows a relatively less CUPRAC antioxidant capacity ($TEAC_{trolox}$ = 1). The low TEAC values of the complex compare to the starting ligand may be described as the consequence of deprotonation of phenolic hydroxyl groups via the template condensation [26].

*3.3.2. Radical scavenging capacity assay (DPPH)*

The 2,2-Diphenyl-1-picrylhydrazyl (DPPH) assayed for the determination of radical scavenging activity of thiosemicarbazone ligand and the Zn(II) complex [70]. DPPH is a stable free radical molecule that is capable of accepting an electron or hydrogen as radical and thus be converted into a stable diamagnetic molecule.

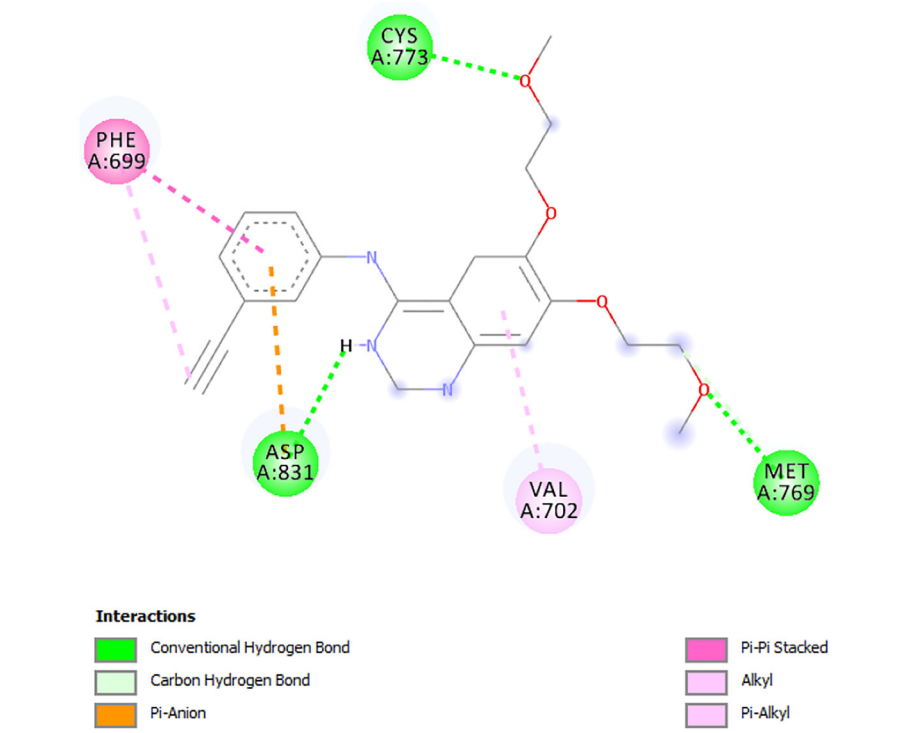


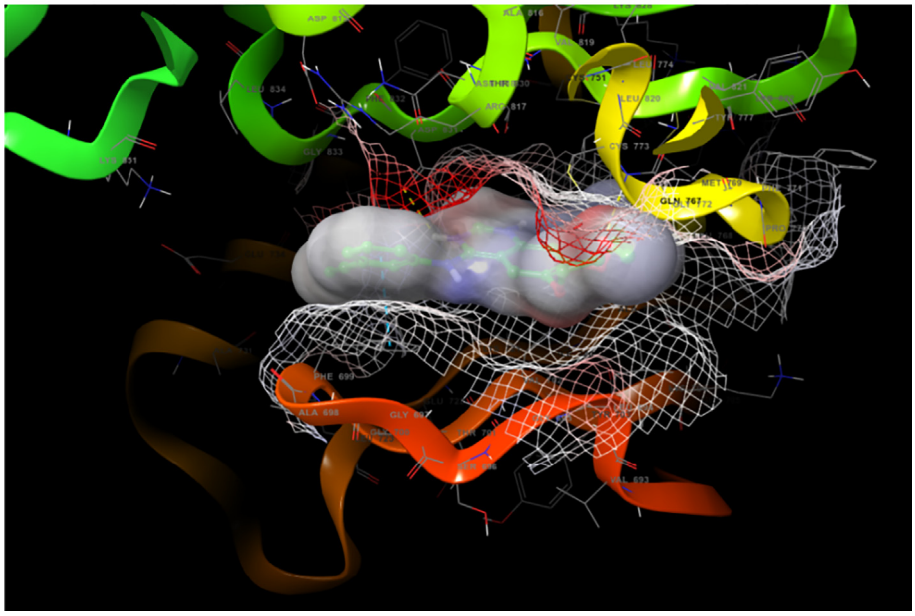

**Fig. 7.** The 3D and 2D presentation of docking results of co-ligand in the active region of the 1 m17 protein.

The odd electron on DPPH donates a strong absorption band at 515 nm. When this odd electron on DPPH paired up, the stoichiometrically decrease in absorption happens with respect to the number of electrons taken up. The radical scavenging activity of the starting ligand (**1**) and Zn(II) complex (**2**) was calculated as percentage inhibition.

The radical scavenging activity for **1** was found as 4.9%, 6.4%, 7.7%, and 11.5% at the concentrations of 50, 100, 150, and 250 μM, respectively. For **2**, the radical scavenging activity was found as 1.91%, 2.13%, and 3.19% at the same concentrations except for the concentration of 250 μM, respectively (Table S2). The Zn(II) complex exhibited relatively low free radical scavenging activity compared to the starting thiosemicarbazone (**1**). This may be due to the lack of free hydroxyl groups and the steric hindrance in the structure [71]. In addition, the radical scavenging activities of both pyridoxal S-methylthiosemicarbazone and its Zn(II) template complex were significantly lower than those of the positive control of ascorbic acid which was agreed with the previous reports that small molecules showed high radical scavenging activities than macromolecules because they were easily accessible to active radicals to provide potential effects in the reaction mixture [26].

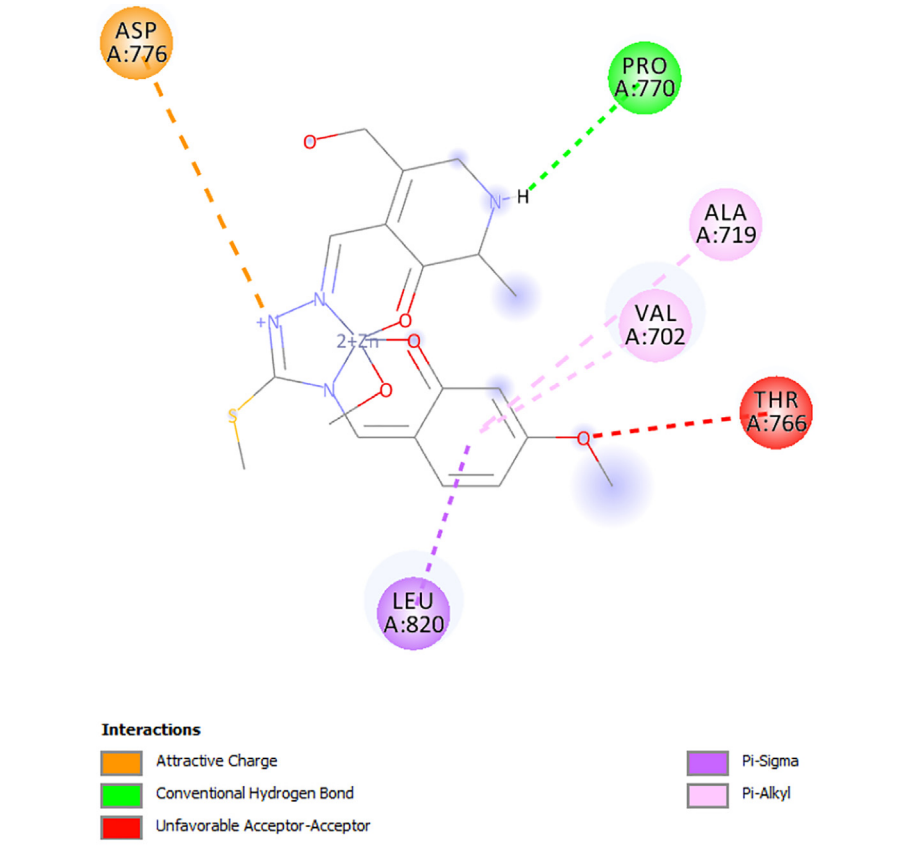


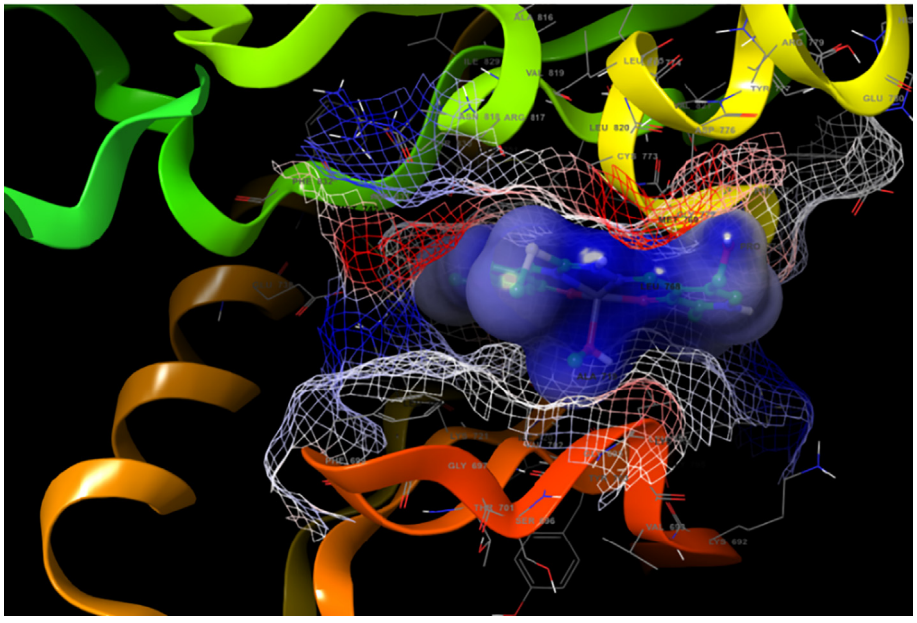

**Fig. 8.** The 3D and 2D presentation of docking results of Zn(II) complex in the active region of the 1 m17 protein.

## 4. Conclusion

In this paper, an unsymmetrical Zn(II) template complex (**2**) of tetradentate $N_2O_2$-type Schiff base ligand derived from pyridoxal-S-methylthiosemicarbazone (**1**) was synthesized for the first time. The starting ligand and Zn(II) complex [Zn(L)$CH_3OH$] were characterized by analytic, spectroscopic, and crystallographic methods. Single crystal X-ray diffraction analysis showed that the complex has a distorted square-pyramidal geometry, and the fifth coordination site is occupied by the oxygen atom of methanol. For the theoretical characterization, the optimized geometries, vibrational frequencies, $^1H$, $^{13}C$ NMR chemical shifts, and electronic characteristics of the compounds were calculated using the DFT method and compared with experimental data. The quantum chemical calculations show good consistency between the predicted and experimental parameters. After the stable structure of the title compound was theoretically calculated, docking simulation was applied to obtain possible bonding models and conformational

structures. The result of the docking obtained showed that the title compound may be a new potential inhibitory agent candidate for the 1 m17 protein structure.

In addition, the synthesized compounds were assayed for antioxidant capacities based on CUPRAC and DPPH methods. As we compared the starting thiosemicarbazone and Zn(II) complex with Trolox (as reference), the TEAC coefficients of the thiosemicarbazone were higher than Trolox ($TEAC_{trolox}$ = 1.0). On the other hand, according to the DPPH assay, the tested compounds showed less free radical scavenging activity compared to ascorbic acid.

## Declaration of Competing Interest

The authors declare that they have no known competing financial interests or personal relationships that could have appeared to influence the work reported in this paper.

## Acknowledgement

We would like to thank to Prof. Bahri Ülküseven for his valuable and continuous support. This paper is a part of PhD thesis of first author.

## Appendix A. Supplementary data

Crystallographic data for the structural analysis has been deposited with the Cambridge Crystallographic Data Centre, CCDC No. 2015478. Copies of this information may be obtained free of charge from the Director, CCDC, 12 Union Road, Cambridge CB2 1EZ, UK (fax: +44-1223-336033; e-mail: deposit@ccdc.cam.ac.uk or www: http://www.ccdc.cam.ac.uk). Supplementary data to this article can be found online at https://doi.org/10.1016/j.poly.2021.115164.

## References

[1] J.S. Casas, M.S. García-Tasende, J. Sordo, Coord. Chem. Rev. 209 (2000) 197–201, https://doi.org/10.1016/S0010-8545(00)00363-5.
[2] E.W. Ainscough, A.M. Brodie, W.A. Denny, G.J. Finlay, J.D. Ranford, J. Inorg. Biochem. 70 (1998) 175–185, https://doi.org/10.1016/S0162-0134(98)10011-9.
[3] N.K. Singh, A.A. Kumbhar, Y.R. Pokharel, P.N. Yadav, J. Inorg. Biochem. 210 (2020), https://doi.org/10.1016/j.jinorgbio.2020.111134 111342.
[4] T. Varadinova, D. Kovala-Demertzi, M. Rupelieva, M. Demertzis, P. Genova, Acta virologica. 45 (2001) 87–94, PMID: 11719987.
[5] L.D. Dave, S.K. Thampy, Y.A. Shelat, J. Inst. Chem. 53 (1981) 237–238.
[6] M. Karatepe, F. Karatas, Cell Biochem. Funct. 24 (2006) 547–554, https://doi.org/10.1002/cbf.1266.
[7] T.S. Lobana, R. Sharma, G. Bawa, S. Khanna, J. Coord. Rev. 253 (2009) 977–1055, https://doi.org/10.1016/j.ccr.2008.07.004.
[8] E.W. Yemeli Tido, C. Faulmann, R. Roswanda, A. Meetsma, P.J. van Koningsbruggen, Dalton Trans. 39 (2010) 1643–1651, https://doi.org/10.1039/B911114J.
[9] M.X. Li, J. Zhou, C.L. Chen, J.P. Wang, Z. Naturforsch. 63 (2014) 280–284, https://doi.org/10.1515/znb-2008-0309.
[10] S.A. Ivković, L.S. Vojinović-Jesić, V.M. Leovac, M.V. Rodić, S.B. Novaković, G.A. Bogdanović, Struct. Chem. 26 (2015) 269–277, https://doi.org/10.1007/s11224-014-0491-6.
[11] E. Littler, B. Oberg, Antivir. Chem. Chemother. 16 (2005) 155–168, https://doi.org/10.1177/095632020501600302.
[12] N.S.H.N. Moorthy, N.M.F.S.A. Cerqueira, M.J Ramos, P.A. Fernandes, Recent Pat. Anti-Canc. 8 (2013) 168–182, https://doi.org/10.2174/1574892811308020005.
[13] E.E. Snell, J. Am. Chem. Soc. 67 (1945) 194–197, https://doi.org/10.1021/ja01218a013.
[14] M. Parra, S. Stahl, H. Hellmann, Cells. 7 (2018) 84–112, https://doi.org/10.3390/cells7070084.
[15] C.C. Hsu, C.H. Cheng, C.L. Hsu, W.J. Lee, S.C. Huang, Y.C. Huang, J. Food Nutr. Res. 59 (2015) 25702–25719, https://doi.org/10.3402/fnr.v59.25702.
[16] M.B. Ferrari, F. Bisceglie, C. Casoli, S. Durot, I.M. Badarau, G. Pelosi, E. Pilotti, S. Pinelli, P. Tarasconi, J. Med. Chem. 48 (2005) 1671–1675, https://doi.org/10.1021/jm049529n.
[17] M.B. Ferrari, F. Bisceglie, E. Leporati, G. Pelosi, P. Tarasconi, Bull. Chem. Soc. Jpn. 75 (2002) 781–788, https://doi.org/10.1246/bcsj.75.781.
[18] M.B. Ferrari, F. Bisceglie, G. Pelosi, P. Tarasconi, R. Albertini, P. Dall'Aglio, S. Pinelli, A. Bergamo, G. Savac, J. Inorg. Biochem. 98 (2004) 301–312, https://doi.org/10.1016/j.jinorgbio.2003.09.011.
[19] D. Kovala-Demertzi, P.N. Yadav, J. Wiecek, S. Skoulika, T. Varadinova, M.A. Demertzis, J. Inorg. Biochem. 100 (2006) 1558–1567, https://doi.org/10.1016/j.jinorgbio.2006.05.006.
[20] A.Y. Louie, T.J. Meade, Chem. Rev. 99 (1999) 2711–2718, https://doi.org/10.1021/cr9804285.
[21] Y. Kurt, A. Koca, M. Akkurt, B. Ülküseven, Inorg. Chim. Acta. 388 (2012) 148–156, https://doi.org/10.1016/j.ica.2012.03.023.
[22] B. Kaya, D. Akyüz, T. Karakurt, O. Şahin, A. Koca, B. Ülküseven, Appl. Organomet. Chem. 34 (2020) e5930–e5942, https://doi.org/10.1002/aoc.5930.
[23] V.M. Leovac, V.I. Cesljevic, N. Galesic, Polyhedron 7 (1988) 2641–2647, https://doi.org/10.1016/S0277-5387(00)83886-3.
[24] B. Ilhan-Ceylan, Inorganica Chim. Acta. 517 (2021) 120186–120195, https://doi.org/10.1016/j.ica.2020.120186.
[25] J. Gradinaru, A. Forni, Yu. Simonov, M. Popovici, S. Zecchin, M. Gdaniec, D.E. Fenton, Inorg. Chim. Acta. 357 (2004) 2728–2736, https://doi.org/10.1016/j.ica.2004.03.008.
[26] B. Kaya, K. Kaya, A. Koca, B. Ülküseven, Polyhedron 173 (2019) 114130–114138, https://doi.org/10.1016/j.poly.2019.114130.
[27] Y. Kurt, N.G. Deniz, J. Coord. Chem. 68 (2015) 4070–4081, https://doi.org/10.1080/00958972.2015.1086760.
[28] V.B. Arion, P. Rapta, J. Telser, S.S. Shova, M. Breza, K. Luspai, J. Kozisek, Inorg. Chem. 50 (2011) 2918–2931, https://doi.org/10.1021/ic102277v.
[29] B. Kaya, Z.K. Yilmaz, O. Şahin, B. Aslim, B. Ülküseven, New. J. Chem. 44 (2020) 9313–9320, https://doi.org/10.1039/D0NJ02149K.
[30] J. Gradinaru, A. Forni, V. Druta, F. Tessore, S. Zecchin, S. Quici, N. Gerbeleu, Inorg. Chem. 46 (2007) 884–895, https://doi.org/10.1021/ic062035r.
[31] R. Apak, K. Güçlü, M. Ozyurek, S.E. Karademir, J. Agric. Food Chem. 52 (2004) 7970–7981, https://doi.org/10.1021/jf048741x.
[32] W. Brand-Williams, M.E. Cuvelier, C. Berset, Lebensem. Wiss. Technol. 28 (1995) 25–30, https://doi.org/10.1016/S0023-6438(95)80008-5.
[33] G.M. Sheldrick, Acta Cryst. A 64 (2008) 112–122, https://doi.org/10.1107/S0108767307043930.
[34] G.M. Sheldrick, Acta Cryst. C 71 (2015) 3–8, https://doi.org/10.1107/S2053229614024218.
[35] Mercury, version 3.3; CCDC, available online via ccdc.cam.ac.uk/products/mercury.
[36] L.J. Farrugia, J. Appl. Cryst. 45 (2012) 849–854, https://doi.org/10.1107/S0021889812029111.
[37] M. Frisch, G. Trucks, H.B. Schlegel, G. Scuseria, M. Robb, J. Cheeseman, G. Scalmani, V. Barone, B. Mennucci, G. Petersson, Gaussian Inc Wallingford CT, Gaussian 09 Revision A. 02 (2009) 200.
[38] A.D. Becke, J. Chem. Phys. 98 (1993) 5648–5652, https://doi.org/10.1063/1.464913.
[39] C. Lee, W. Yang, R.G. Parr, Phys. Rev. B. 37 (1988) 785–789, https://doi.org/10.1103/physrevb.37.785.
[40] J.B. Foresman, S. Frisch, Exploring chemistry with electronic structure methods: a guide to using Gaussian, Gaussian, Inc, 1996.
[41] P.J. Hay, W.R. Wadt, J. Chem. Phys. 82 (1985) 270–283, https://doi.org/10.1063/1.448799.
[42] P.J. Hay, W.R. Wadt, J. Chem. Phys. 82 (1985) 299–310, https://doi.org/10.1063/1.448975.
[43] W.R. Wadt, P.J. Hay, J. Chem. Phys. 82 (1985) 284–298, https://doi.org/10.1063/1.448800.
[44] M. H. Jamróz, Vibrational Energy Distribution Analysis VEDA 4, Warsaw (2004).
[45] S. Dallakyan, A.J. Olson, Methods, Mol. Biol. 1263 (2015) 243–250, https://doi.org/10.1007/978-1-4939-2269-7_19.
[46] O. Trott, A.J. Olson, J. Comput. Chem. 31 (2010) 455–461, https://doi.org/10.1002/jcc.21334.
[47] Dassault Systemes BIOVIA, Discovery Studio Modeling Environment, Release20.1, San Diego, 2020
[48] V.M. Leovac, V.S. Jevtovic, G.A. Bogdanovic, Acta. Cryst. 58 (2002) 514–516, https://doi.org/10.1107/S010827010201586X.
[49] J.B. Foresman, A. Frisch, Exploring Chemistry with Electronic Structure Methods, second ed., Gaussian Inc, Pittsburgh, 1996.
[50] M.F. Belicchi, G.F. Gasparri, E. Leporati, C. Pelizzi, P. Tarasconi, G. Tosi, J. Chem. Soc., Dalton Trans. 11 (1986) 2455–2461, https://doi.org/10.1039/DT9860002455.
[51] V.M. Leovac, V. Divjaković, M. Joksović, L. Jovanović, L. Vojinović-Ješić, V. Češljević, M. Milinar, J. Serb. Chem. Soc. 75 (2010) 1063–1074, https://doi.org/10.2298/JSC100113045L.
[52] D. Heinert, A.E. Martell, J. Am. Chem. Soc. 81 (1959) 3933–3943.
[53] B. Ilhan-Ceylan, O. Bolukbasi, A. Yilmaz, K. Kaya, Y. Kurt, B. Ülküseven, Polyhedron 193 (2021) 114884–114893, https://doi.org/10.1016/j.poly.2020.114884.
[54] H. Bahron, S.S. Khaidir, A.M. Tajuddin, K. Ramasamy, B.M. Yamin, Polyhedron 161 (2019) 84–92, https://doi.org/10.1016/j.poly.2018.12.055.
[55] M. Mohan, P.H. Madhuranath, A. Kumar, M. Kumar, N.K. Jha, Inorg. Chem. 28 (1989) 96–99, https://doi.org/10.1021/ic00300a022.
[56] R. Ditchfield, J. Chem. Phys. 56 (1972) 5688–5691, https://doi.org/10.1063/1.1677088.
[57] P. Pulay, K. Wolinski, J. Hinton, J. Am. Chem. Soc. 112 (1990) 8251–8260, https://doi.org/10.1021/ja00179a005.

[58] S.A. Abdel-Latif, A.A. Mohamed, J. Mol, Struct. 1153 (2018) 48–261, https://doi.org/10.1016/j.molstruc.2017.10.002.
[59] K. Fukui, Science. 218 (1982) 747–754, https://doi.org/10.1126/science.218.4574.747, PMID: 17771019.
[60] H. Buyukuslu, M. Akdogan, G. Yildirim, C. Parlak, Spectrochim. Acta A. 75 (2010) 1362–1369, https://doi.org/10.1016/j.saa.2010.01.003.
[61] R.G. Parr, R.G. Pearson, J. Am. Chem. Soc. 105 (1983) 7512–7516, https://doi.org/10.1021/ja00364a005.
[62] R.G. Parr, R.A. Donnelly, M. Levy, W.E. Palke, J. Chem. Phys. 68 (1978) 3801–3807, https://doi.org/10.1063/1.436185.
[63] R.G. Parr, L.V. Szentpály, S. Liu, J. Am. Chem. Soc. 121 (1999) 1922–1924, https://doi.org/10.1021/ja983494x.
[64] M. Tümer, Synth. React. Inorg M. 41 (2011) 211–223, https://doi.org/10.1080/15533174.2010.538288.
[65] C.M. Sharaby, Spectrochim. Acta A. 66 (2007) 1271–1278, https://doi.org/10.1016/j.saa.2006.05.030.
[66] P. Jain, V. Singh, S. Ali, V. Tripathi, U. Saraswat, J. Saudi Chem. Soc. 22 (2018) 546–557, https://doi.org/10.1016/j.jscs.2017.09.005.
[67] T. Mitsudomi, Y. Yatabe, FEBS J. 277 (2010) 301–308, https://doi.org/10.1111/j.1742-4658.2009.07448.x.
[68] S. Kalyankrishna, J.R. Grandis, J. Clin. Oncol. 24 (2006) 2666–2672, https://doi.org/10.1200/JCO.2005.04.8306.
[69] J. Morrison, K. Haldar, S. Kehoe, T.A. Lawrie, Cochrane Database of Systematic Reviews 8 (2012), https://doi.org/10.1002/14651858.CD005343.pub3.
[70] B. Ilhan-Ceylan, E. Tüzün, Y. Kurt, M. Acikgoz, S. Kahraman, G. Atun, B. Ulkuseven, J. Sulphur. Chem. 36 (2015) 434–449, https://doi.org/10.1080/17415993.2015.1050396.
[71] D. Villaño, M.S. Fernández-Pachón, M.L. Moyá, A.M. Troncoso, M.C. García-Parrilla, Talanta. 71 (2007) 230–235, https://doi.org/10.1016/j.talanta.2006.03.050.